Mechanical Systems and Signal Processing 151 (2021) 107440

Contents lists available at ScienceDirect

Mechanical Systems and Signal Processing

journal homepage: www.elsevier.com/locate/ymssp

System-level finite element analysis of piezoelectric energy harvesters with rectified interface circuits and experimental validation

Feng Qian [a], Yabin Liao [b,*], Lei Zuo [a], Phil Jones [b]

[a] Department of Mechanical Engineering, Virginia Polytechnic Institute and State University, Blacksburg, VA 24061, USA
[b] Department of Mechanical Engineering Technology, Pennsylvania State University – Erie, Erie, PA 16563, USA

ARTICLE INFO

Article history:
Received 21 July 2020
Received in revised form 23 September 2020
Accepted 7 November 2020
Available online 20 November 2020

Keywords:
Energy harvesting
Piezoelectric
AC-DC
Equivalent circuit
Finite element
ANSYS

ABSTRACT

The finite element method (FEM) has been widely used for numerical studies of piezoelectric energy harvesting (PEH) systems, through commercial finite element (FE) packages or specially developed FE formulations. As a convenient computational tool, FEM can deal with systems of high complexity and has evolved into a multiphasic solution to coupled problems in engineering. However, most of FE packages and formulations are limited to coupled-field simulations of PEH systems connected with a linear circuit. On the other hand, rectified circuits are a critical component in practical applications because electronic devices such as wireless sensor nodes and wearable electronics require a DC power supply. Based on the equivalent impedance analysis, this paper proposes a method to enable a coupled-field study of piezoelectric energy harvesters with the standard AC-DC interface circuit through an equivalent linear circuit. The proposed method enables FE packages and formulations to analyze, design, and optimize PEH harvesters at the system level, by either adding the capability of simulating rectified circuits, or reducing a nonlinear circuit interface simulation into a faster and more stable linear simulation that can be solved more conveniently. This equivalent linear circuit method was applied to a rectangular shaped bimorph beam harvester in ANSYS and validated experimentally. The results also match well with those obtained from a system-level analytical approach. As an application example, a comparison study was performed between the rectangular and triangular energy harvesters using FE packages and the proposed equivalent circuit, given the same natural frequency and material volume. In addition, the implementation of this method with FE formulations is briefly outlined and discussed.

1. Introduction

Wireless sensor networks (WSNs) have become more desirable with the rapid advance of emerging applications such as Internet of Things (IoT), autonomous systems, robotics, smart cities, and wearable electronics. However, sustainable power supply is a long-stand challenge for WSNs. They are mostly powered by chemical batteries with a finite lifetime that require regular replacement or recharging. Therefore, self-powered capability is critical for wireless sensor nodes. Piezoelectric energy harvesting (PEH) appears to be a viable solution to this end [1]. The direct piezoelectric effect produces electric

* Corresponding author.
E-mail address: Yabin.Liao@psu.edu (Y. Liao).

https://doi.org/10.1016/j.ymssp.2020.107440
0888-3270/

charges from mechanical strains caused by ambient vibrations. This inherent effect of piezoelectric materials makes it possible for the energy harvesting component to have a compact and simple architecture, facilitating its integration with wireless sensor networks. Significant advances in PEH have been accomplished in the past two decades, resulting in a much deeper and broader understanding in multiple aspects such as structural dynamics, materials, and electrical circuitry. A summary of these developments can be found in review articles [2–7].

During the course of these research efforts in PEH, many analytical or approximate solutions have been obtained. However, they are applicable only to configurations with simple geometric shapes, boundary conditions, and load conditions. It is indispensable to utilize numerical tools such as finite element method (FEM) to deal with systems of more complexity, validating theoretical formulations, providing perspectives on system behaviors, and offering design guidance. For this purpose, commercial finite element analysis (FEA) packages have been commonly used. As a convenient computational tool, they can deal with complex systems and have evolved into a multiphasic solution to coupled problems in engineering. However, most FEA packages have limited capabilities as to the modeling of piezoelectric energy harvesting systems, whose dynamics are electromechanically coupled. For example, ABAQUS allows direct simulation of piezoelectric elements but cannot model a fully coupled electromechanical system because of unavailable electric circuit simulations [8]. NASTRAN does not have the capability of modeling piezoelectricity. It can simulate actuation dynamics based on a thermal-to-piezoelectric analogy [8,9] but still cannot perform a fully coupled simulation due to the lack of electrical circuitry component [8]. On the other hand, ANSYS has been recognized as the most commonly used commercial FEA package for PEH due to its built-in piezoelectricity feature that can model the fully coupled field. In addition, it offers efficient solvers and strong meshing capabilities, along with a powerful ANSYS Parametric Design Language (APDL) for advanced users to parameterize the model and automate tasks. Zhu et al [10] firstly conducted the FEA analysis using ANSYS on a piezoelectric cantilever energy harvester with a simple circuit connected to a load resistor. Recently, Kuang and Zhu [11] used the similar piezoelectric-circuit model to study the energy harvesting from mechanical plucking vibration and experimentally validated the model. Yang and Tang [12] derived the system parameters of a piezoelectric cantilever energy harvester from the ANSYS FE analysis for a multimode equivalent circuit model to perform the electromechanical coupling analysis. For conventional vibration energy harvesters of a cantilever configuration, Arafa et al. [13] proposed the concept of dynamic magnification of the base motion at the fixed end by placing a spring-mass system between the fixed end of the piezoelectric beam and the vibrating base structure. They performed an experimental demonstration of the concept and conducted validation studies using ANSYS simulations. Bai et al. [14] developed a linear kinetic energy harvester for energy harvesting from human motion. The harvester had a piezoelectric cantilever with a tip mass, and utilized the motion of wrist and head spin. ANSYS simulations were used to aid their conceptual designs and optimization of system parameters. Qian et al. [15] modeled a piezoelectric stack-based boot energy harvester shunted to a resistor in ANSYS and experimentally validated the model. They also developed a material equivalent model to handle the mesh problem of the very thin piezoelectric layers in the stack. Wang et al. [16] proposed an energy harvesting type piezoelectric ultrasonic actuator that had a sandwich-type stator composed of a metal body, an exciting PZT ring used to produce a traveling wave, and a harvesting PZT ring to convert and harvest the vibration-induced energy of the stator. They performed design studies for optimal structural parameters and conducted harmonic and transient energy harvesting simulations using ANSYS. Li et al. [17] proposed a generalized multi-mode PEH that consists of a main cantilevered beam attached with multiple branches with tip masses. The structure can be configured to generate close multiple resonance peaks within a frequency range, making it suitable for broadband energy harvesting. They developed the analytical model for the system, and validated it through ANSYS simulations. Other examples of using ANSYS coupled-field simulations for design optimization and numerical validation of PEH systems include [18–21], just to name a few.

In addition to commercial FEA packages, researchers also have developed their own FE formulation to model PEH systems. De Marqui et al. [22] presented an electromechanically coupled finite element (FE) formulation for predicting harvested power of piezoelectric energy harvester plates. The formulation was derived based on the generalized Hamilton's principle and the Kirchhoff assumptions for thin plates. Kumar et al. [23] developed a finite element formulation to model unimorph cantilever type PEH harvesters. The formulation applied the first-order shear deformation theory to account for the shear effect of the structure in the thickness direction. Fattahi and Mirdamadi [24] derived a general finite element formulation using generalized Hamilton's principle based on 3D active beam elements, and the equivalent layer theory in both the mechanical and electrical domains. Ramírez et al. [25] proposed a one-dimensional finite element formulation to model 3D rotational PEH devices based on geometrically nonlinear elements. Timoshenko beam theory was used in the mechanical domain to obtain the dynamics of a rotating beam. Recently, to perform parametric uncertainty analysis of PEH systems, Wang et al. [26] applied a FE formulation in NASTRAN through the thermal-piezoelectric analogy, which made it possible to add uncertainties at an element level. In addition, Amini et al. [27] and Ravi and Zilian [28] developed FE formulations to investigate PEH from fluid-structure interaction.

A great amount of valuable information was obtained from FE simulations in those aforementioned examples, either through commercial FE package or custom developed FE formulations. However, the adopted external energy harvesting interface circuit was resistive, i.e., the piezoelectric elements were simply connected to a resistor. While it is a reasonable configuration for theoretical development and modeling of PEH systems, practical electronic devices such as wireless sensor nodes and wearable electronics require a DC power supply. For this purpose, the direct AC power generated by piezoelectric energy harvesters needs to be rectified. The simplest way to achieve this is through a full-bridge AC-DC rectifier, which is usually connected with a large capacitor to reduce the ripple in the output voltage signal to the electrical load.

This configuration is called the standard energy harvesting (SEH) interface scheme. Ottman et al. [29] developed an energy harvesting circuit that consisted of an AC-DC rectifier with an output capacitor, and a switch-mode DC-DC converter to charge an electrochemical battery. An adaptive control technique for the DC-DC converter was implemented to maximize the power stored by the battery. Guyomar et al. [30] performed an analytical analysis of the SEH circuit interface, and proposed the Synchronized Switch Harvesting on Inductor (SSHI) circuit interface, which was originally developed by Richard et al. [31] for shunt damping applications, for energy harvesting to improve the power harvesting performance, especially for lowly coupled systems. Ramadass and Chandrakasan [32] proposed a bias-flip rectifier circuit to improve the power extraction of capability over conventional full-bridge rectifiers. An efficient control circuit with embedded DC-DC converters was used to regulate the output voltage of the rectifier, and had a filter inductor shared with the rectifier to reduce the overall volume and component count. Motter et al. [33] evaluated and compared the experimental results and numerical results of a PEH with a standard AC-DC interface circuit. They also provided few practical considerations on the selection of capacitance and resistance loads. Mustapha et al. [34] performed numerical and experimental studies on the harvested power and AC-DC conversion efficiency with various types of diodes in a standard AC-DC circuit interface configuration, including conventional diode (1 N4001), Zener diode (1 N750), Schottky diode (BAT754), MOSFET full bridge rectifier and an active rectifier. The active rectifier using MOSFET switching operation were found to have a better conversion efficiency than passive rectifiers. Dicken et al. [35] proposed a unified analytical framework to analyze and compare PEH interface circuits including the standard AC-DC, S-SSHI, P-SSHI, and pre-biasing rectified circuits. Their analysis included the effect of fixed on-state voltage drop of the diode. Szarka et al. [36] reviewed passive and active rectification techniques such as the conventional full-bridge rectifier, diode-tied MOS rectifier, gate cross-coupled NMOS rectifier, cross-coupled rectifier, and active rectifier with cross-coupled PMOS switches. As in practical situations, output voltage must be regulated to meet the requirements of load devices, they also reviewed voltage conditioning techniques, for instance, voltage multipliers and DC-DC converters.

Though rectified circuits are of great value to practical energy harvesting applications, most available FE programs, either commercial packages or developed formulations, do not have the direct capability of performing electromechanically coupled simulations of PEH systems with rectified circuits. For instance, PEH simulations in ANSYS are limited to linear circuit elements such as resistors, capacitors and inductors. To circumvent this issue, some researchers resorted to a two-step process based on the equivalent circuit analysis, which converts the vibration excitation into either a voltage or current source, and the effective system quantities such as mass, stiffness and damping are analogous to source inductance, capacitance and resistance, respectively. Next, circuit simulators such as PSpice and Simulink are used for simulation studies. The source quantities can be assumed [37], obtained by using analytical formulations, experimentally determined from measurements [38], or estimated from FEA [12,39]. This approach is a reasonable option if the focus is on the energy harvesting circuitry, but not desirable for design and optimization studies at a system level for PEH systems whose dynamics are coupled in both mechanical and electrical domains. Moreover, the analytical formulations used to obtain the source quantities are limited by the complexity of the system and assumptions on their underlying theories. In addition, estimating the source quantities experimentally or from a separate FE simulation increases the overall efforts and possibility for errors. Given these reasons, Wu and Shu [40] proposed a method to realize a direct simulation with rectified circuitry at a system level for FE packages. They replaced the external energy harvesting circuit with an equivalent impedance load in parallel with a negative capacitor, i.e., active element relying on an external power source, which cancels the internal piezoelectric capacitance of the system. The concept of equivalent impedance for PEH systems was proposed by Liang and Liao [38], where the effect of the energy harvesting interface circuit and internal piezoelectric capacitance is represented by an electrical equivalent impedance load. They used it to build equivalent linear impedance networks for PEH systems with different interface circuits and study the power optimization from an impedance perspective. Cheng et al. [41] made an another attempt, using an equivalent impedance load to directly approximate the nonlinear dynamics of a P-SSHI interface circuit. However, the impedance was not explicitly given in terms of the electrical load, making it inconvenient for implementation.

The main contribution of the paper is to propose and experimentally validate a method that enables a direct, full coupled-field study of piezoelectric energy harvesters with rectified interface circuits through an equivalent passive linear circuit. It opens up opportunities for FE packages in the fast analysis, design, and optimization of PEH harvesters with complex geometry at a system level with more practical energy harvesting interface circuits. The main idea, as illustrated in Fig. 1, is to use an equivalent linear circuit of two passive elements in series (in the dashed box) to represent the original nonlinear interface circuit. One of the elements is resistive and the other one could be capacitive or inductive depending on the type of the original rectified circuit and system parameters. The concept of equivalent impedance is used to obtain the equivalent linear circuit. This concept was recently used by Liao and Liang to study the relationship between the electromechanical coupling and harvested power of PEH systems in [42], and then build a unified model of PEH systems with various energy harvesting interface circuits in [43]. The advantages of this proposed method, as compared to the methods in [40,41], include that the use of passive instead of active elements provides more physical insights on the circuit equivalency, and the values of equivalent linear elements are explicitly given in terms of the electrical load, excitation frequency, and intrinsic piezoelectric capacitance of the system, making its implementation convenient in practical design applications.

For validation, the method is applied to a fully covered piezoelectric bimorph beam connected with a standard full-bridge AC-DC circuit and the analytical, FE, and experimental results are compared. The analytical results are obtained through an integration of two validated models developed by Shu and Lien in [37] and Liao and Sodano in [44], respectively. The effective lumped single-degree-of-freedom (SDOF) system parameters of beam PEHs were given by Liao and Sodano in closed-form in [44], along with experimental validation on a bimorph PEH connected with an AC circuit. An analytical power

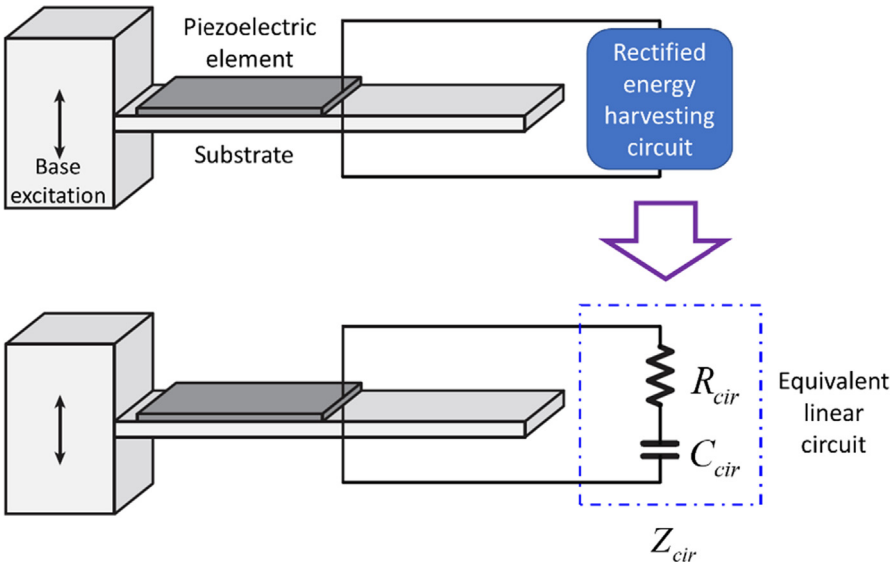

Fig. 1. Schematic of a piezoelectric energy harvester with a rectified circuit and the equivalent external linear circuit.

expression of piezoelectric energy harvesters connected with an AC-DC circuit was presented by Shu and Lien [37], given measured or analytically determined effective lumped system parameters. However, it cannot directly deal with PEH systems of complex geometries, for which the closed-form expression of lumped system parameters might be unattainable. Nevertheless, the proposed FE-equivalent-circuit method does not have this limitation. The equivalency of the circuitry is independent of the mechanical or structural aspect of the system; while FE methods are more than capable of modeling the mechanical aspect of electromechanical systems of complex geometries. Therefore, the proposed method can be applied to systems of complex geometry as well.

The rest of the paper is organized as follows. In Section 2, the concept of equivalent electrical impedance is discussed, and the equivalent linear circuit characteristics will be extracted from the electrical impedance of the system. In Section 3, a bimorph beam energy harvester is modeled in ANSYS and analyzed by the proposed equivalent linear circuit method. Experiments and the system-level analytical analysis based on two analytical models are conducted to validate the ANSYS results. As an application example, Section 4 presents an ANSYS-based comparison study of the power characteristics of a rectangular harvester and a triangular harvester connected to a standard AC-DC interface circuit and studies the effect of electromechanical coupling on the results. Finally, the implementation of this proposed method in FE formulations is briefly outlined and discussed in Section 5.

2. Equivalent external linear circuit analysis

To determine the characteristics of the equivalent external linear circuit, this section starts with a brief overview of the equivalent impedance concept for piezoelectric energy harvesters. Then the equivalent electrical impedance of AC-DC interface circuits is discussed, from which the impedance of the equivalent linear circuit is extracted. After that, the types and values of the equivalent passive circuit elements, i.e., resistor, capacitor, or inductor, are determined based on the extracted circuit impedance.

2.1. Equivalent circuit and impedance of a general piezoelectric energy harvester

In general, the electromechanically coupled dynamics of a piezoelectric vibration energy harvester subjected to a base acceleration excitation can be simply modelled as a single-degree-of-freedom (SDOF) system described by the following equations [44,45]:

$$\begin{cases} M\ddot{w}(t) + C\dot{w}(t) + Kw(t) - \theta v_p(t) = Da(t) \\ \theta w(t) + C_p v_p(t) = q(t) \end{cases}. \tag{1}$$

where $w(t)$ and $v_p(t)$ are the displacement and voltage responses of the SDOF system, $a(t)$ is the excitation acceleration, and q (t) the electric charge over the piezoelectric element. M, C, K, θ are the effective mass, damping coefficient, stiffness, and electromechanical coupling coefficient. D is an equivalent mass multiplied with acceleration $a(t)$ to represent the equivalent external force applied to the SDOF system.

The two governing equations can be manipulated to yield an equivalent circuit [38] based on the analogy between the mechanical domain and electric domain as shown in Fig. 2. In this way, the entire system can be analyzed in the electrical domain alone, thus simplifies the analysis process, and offers a better view of the connection between system components. The equivalent circuit quantities are related to the original mechanical system parameters as

$$v_{eq}(t) = -\frac{D}{\theta}a(t), i_{eq}(t) = -\theta\dot{w}(t), i_p = -\dot{q}(t) \tag{2}$$

where the acceleration excitation acts as a voltage source and the structural velocity acts as the induced current equivalently. The electrical elements of the equivalent circuit are obtained as

$$L_s = \frac{M}{\theta^2}, R_s = \frac{C}{\theta^2}, C_s = \frac{\theta^2}{K}. \tag{3}$$

The *circuit impedance* Z_{cir} in the shaded area of Fig. 2 represents the energy harvesting interface circuit. The *electrical impedance* Z_{elec} represents the electrical aspect of the system, combining both the internal capacitance C_p of the piezoelectric elements and the circuit impedance Z_{cir}. For linear energy harvesting circuits, Z_{elec} can be obtained directly and exactly. For nonlinear energy harvesting circuits, e.g., SEH and SSHI interfaces, an equivalent electrical impedance can be used to approximate the nonlinear dynamics of the circuit [38,40].

Consider a generalized electrical impedance Z_{elec} (either exact or equivalent) is used to represent the shaded area in Fig. 2. The harvested power can be obtained by first expressing Z_{elec} in its component form as

$$Z_{elec} = R_{elec} + jX_{elec}, \tag{4}$$

where R_{elec} and X_{elec} are the resistive and reactive components, respectively. Then applying basic circuit theories to the system with harmonic base excitation of amplitude A and frequency ω yields the AC power (or equivalent AC power in the case of a rectified circuit) extracted or dissipated in the resistive component of the energy harvesting interface circuit:

$$P = \frac{D^2A^2}{\sqrt{MK}} \frac{k^2r^2\gamma}{\left(2\zeta r + k^2r\gamma\right)^2 + \left(1 - r^2 - k^2r\chi\right)^2}, \tag{5}$$

where $\zeta = \frac{C}{2\sqrt{KM}}$ is the mechanical damping ratio, and the dimensionless electrical resistance and reactance are defined as

$$\gamma = \omega_n C_p R_{elec}, \chi = \omega_n C_p X_{elec} \tag{6}$$

The short-circuit natural frequency ω_n, frequency ratio r and effective electromechanical coupling coefficient k^2 are defined as

$$\omega_n = \sqrt{\frac{K}{M}}, r = \frac{\omega}{\omega_n}, k^2 = \frac{\theta^2}{C_pK}. \tag{7}$$

2.2. Equivalent linear circuit of a standard AC-DC interface circuit

Fig. 3 shows the schematic of a standard energy harvester (SEH) with an AC-DC rectifier, where R is the electrical load resistance and C_e is a large capacitor used to smooth out the voltage signal after the rectification. The closed-form power expression given by Shu and Lien [37] as

$$P_{SEH} = \frac{D^2A^2}{\sqrt{MK}} \frac{\frac{2k^2r^2\rho}{(r\rho+\pi/2)^2}}{\left\{2\zeta r + \frac{2k^2r\rho}{(r\rho+\pi/2)^2}\right\}^2 + \left\{1 - r^2 + \frac{k^2r}{r\rho+\pi/2}\right\}^2}, \tag{8}$$

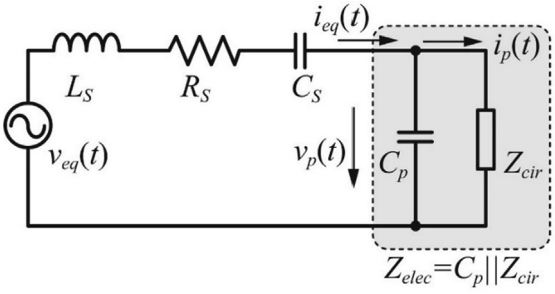

Fig. 2. Equivalent circuit of a piezoelectric energy harvester subjected to a base excitation.

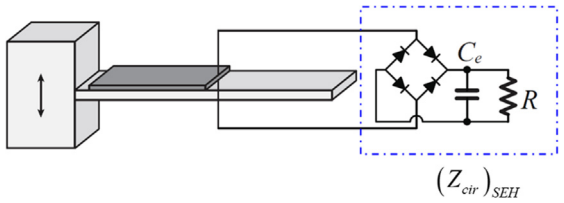

Fig. 3. Schematic of a standard energy harvester (SEH) with an AC-DC rectifier.

where the dimensionless resistance

$$\rho = \omega_n C_p R. \tag{9}$$

Note that expression (8) gives an equivalent AC power. The actual DC power output of the standard AC-DC circuit is half of the equivalent AC power. By comparing the power Expression (5) of the generalized model reveals that for the SEH interface, the dimensionless equivalent impedance components are [43]:

$$\gamma_{SEH} = \frac{2\rho}{(r\rho + \pi/2)^2}, \chi_{SEH} = -\frac{\rho}{r\rho + \pi/2}. \tag{10}$$

Based on these dimensionless results, along with Eqs. (4), (6), (9), the equivalent electrical impedance of the SEH interface can be written as

$$(Z_{elec})_{SEH} = \frac{2R}{(\omega C_p R + \pi/2)^2} - j\frac{R}{\omega C_p R + \pi/2}, \tag{11}$$

which is a function of the excitation frequency ω and electrical load R. Note this electrical impedance Z_{elec} includes both the external energy harvesting circuit impedance Z_{cir} and the internal piezoelectric capacitance C_p as shown by the shaded area in Fig. 2.

The same expression was obtained by Lien and Shu [46] following a different approach. Instead of comparing the power expressions, they compared the denominator of the structural response expression obtained in [37] with that based on the generalized electrical impedance. Additionally, Liang and Liao [38] also derived an expression for $(Z_{elec})_{SEH}$ based on Fourier approximation. However, it was given in terms of the rectifier blocked angle in a half cycle, not the electrical load explicitly.

In this paper, the external circuit impedance Z_{cir} is obtained from the electrical impedance Z_{elec} as follows. Firstly, express the circuit impedance in the component form

$$Z_{cir} = R_{cir} + jX_{cir}. \tag{12}$$

By noting that the electrical impedance is the combination of the external circuit impedance and internal piezoelectric capacitance in parallel, we have

$$Z_{elec} = Z_{C_p} || Z_{cir} = \frac{Z_{C_p} Z_{cir}}{Z_{C_p} + Z_{cir}} = \frac{R_{cir} - j\left(\omega C_p R_{cir}^2 + \omega C_p X_{cir}^2 - X_{cir}\right)}{\left(\omega C_p R_{cir}\right)^2 + \left(\omega C_p X_{cir} - 1\right)^2}, \tag{13}$$

where "||" denotes the parallel connection of electrical elements and Z_{Cp} is the impedance of the internal capacitance, i.e., $Z_{Cp} = 1/(\omega C_p)$. After that, equating Equations (11) and (13), separating the real and imaginary components, and flipping the numerators and denominators on both sides (for manipulation conveniences) yield two coupled equations for the circuit impedance components R_{cir} and X_{cir}:

$$\frac{\left(\omega C_p R_{cir}\right)^2 + \left(\omega C_p X_{cir} - 1\right)^2}{R_{cir}} = \frac{\left(\omega C_p R + \pi/2\right)^2}{2R}, \tag{14}$$

$$\frac{\left(\omega C_p R_{cir}\right)^2 + \left(\omega C_p X_{cir} - 1\right)^2}{\omega C_p R_{cir}^2 + \omega C_p X_{cir}^2 - X_{cir}} = \frac{\omega C_p R + \pi/2}{R}. \tag{15}$$

Dividing Eq. (14) by (15) on both sides yields

$$\frac{\omega C_p R_{cir}^2 + \omega C_p X_{cir}^2 - X_{cir}}{R_{cir}} = \frac{\omega C_p R + \pi/2}{2}. \tag{16}$$

The second-order terms of R_{cir} and X_{cir} can be removed by multiplying both sides of Eq. (16) with ωC_p and subtracting Equation (14) from the result, yielding a linear relationship between R_{cir} and X_{cir}:

$$\omega C_p X_{cir} - 1 = -\frac{\pi(\omega C_p R + \pi/2)}{4R} R_{cir}. \tag{17}$$

Substituting this result back into Equation (14) yields an equation for R_{cir} only. Solve the equation and we have:

$$(R_{cir})_{SEH} = \left\{ \frac{1}{2} \frac{(\omega C_p R + \pi/2)^2}{(\omega C_p R)^2 + (\pi/4)^2 (\omega C_p R + \pi/2)^2} \right\} R. \tag{18}$$

Substituting it back into Equation (17) yields

$$(X_{cir})_{SEH} = \left\{ \frac{\omega C_p R - (\pi/8)(\omega C_p R + \pi/2)^2}{(\omega C_p R)^2 + (\pi/4)^2 (\omega C_p R + \pi/2)^2} \right\} R. \tag{19}$$

Similar to the electrical impedance given in Eq. (11), the circuit impedance components also depend on the load resistance R, piezoelectric capacitance C_p and excitation frequency ω. The effect of capacitance and frequency is applied in the form of the product $\omega C_p R$. As an example, Fig. 4 plots the closed-form results of R_{cir} and X_{cir} given by Eq. (18) and (19) for a fixed load of R = 5616 Ω over the frequency range of 110–160 Hz with C_p = 0.136 μF, which matches the testing setting of an actual bimorph energy harvester [44].

An alternate approach to determining the equivalent circuit impedance Z_{cir} (and its R_{cir} and X_{cir} components) is to solve for Z_{cir} from the impedance relationship

$$\frac{1}{Z_{elec}} = \frac{1}{Z_{C_p}} + \frac{1}{Z_{cir}}, \tag{20}$$

which gives

$$Z_{cir} = \frac{Z_{C_p} - Z_{elec}}{Z_{C_p} Z_{elec}}. \tag{21}$$

It can be shown that substituting the electrical impedance of the SEH interface, i.e., Eq. (11), and the impedance of the internal capacitance into (21) yields the same results as in Eqs. (18) and (19).

Once the equivalent circuit impedance components R_{cir} and X_{cir} have been determined, the next step is to find the corresponding linear electrical elements in the equivalent external circuit (refer to Fig. 1). The resistive impedance component R_{cir} can be simply represented by a resistor directly. To find a suitable passive element for the reactance component X_{cir}, the reactance type needs to be determined, i.e., capacitive or inductive. This can be done by noting that the denominator of expression (19) is always positive, and the numerator can be manipulated and rewritten as

$$-\frac{\pi}{8}\left(\omega C_p R + \frac{\pi}{2} - \frac{4}{\pi}\right)^2 - \frac{\pi}{2} + \frac{2}{\pi}, \tag{22}$$

which is always negative because of the negative sign in front of the squared expression and the additional fact that $2/\pi$ is smaller than $\pi/2$. Therefore, the reactance component X_{cir} is always negative as graphically shown in Fig. 4(b), and it is a capacitive reactance equivalently. The capacitance of the capacitor used to represent X_{cir} in the equivalent external circuit is

$$(C_{cir})_{SEH} = -\frac{1}{\omega X_{cir}} = \frac{1}{\omega R} \left\{ \frac{(\omega C_p R)^2 + (\pi/4)^2 (\omega C_p R + \pi/2)^2}{-\omega C_p R + (\pi/8)(\omega C_p R + \pi/2)^2} \right\}. \tag{23}$$

For illustration purposes, Fig. 5 plots the capacitance of the equivalent capacitor associated with X_{cir} in Fig. 4(b). It can be seen that the capacitor is a variable capacitor with respect to frequency, similar to the equivalent external circuit resistor as shown in Fig. 4(a).

3. Experiments and results

3.1. Experimental setup

For validation, this equivalent linear circuit method was applied to a bimorph beam energy harvester with properties given in Table 1. It consisted of two same-size PZT-5A4E layers and a middle brass layer. The two PZT elements were connected in parallel electrically. One end of the composite beam was free and a base excitation of 0.5 m/s^2 was exerted by a VG-100 electromagnetic shaker at the other end fixed to the base. The mechanical damping ratio was determined to be 0.0115 using the log decrement method from the measured free response of the system. Fig. 6 (a) shows the picture of the overall experimental setup, where the Spider 80X dynamic analyzer (Crystal Instruments) was used to generate the excitation signal and collect data. The generated signal was amplified by the amplifier (HAS 4051, NF Corporation) before fed to the shaker to achieve the expected base excitation acceleration. The piezoelectric bimorph energy harvester was clamped by a fixer installed on the shaker, as shown in the close-up view in Fig. 6 (b). The excitation acceleration of the shaker was monitored

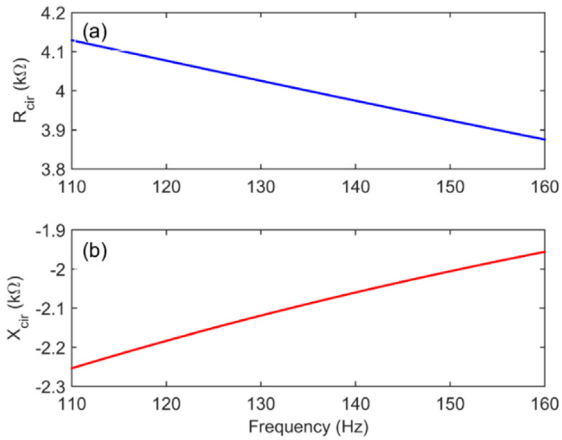

Fig. 4. Equivalent external linear circuit impedance components R_{cir} and X_{cir} obtained from Eqs. (18) and (19). Fixed load R = 5616 Ω, piezoelectric capacitance C_p = 0.136 μF.

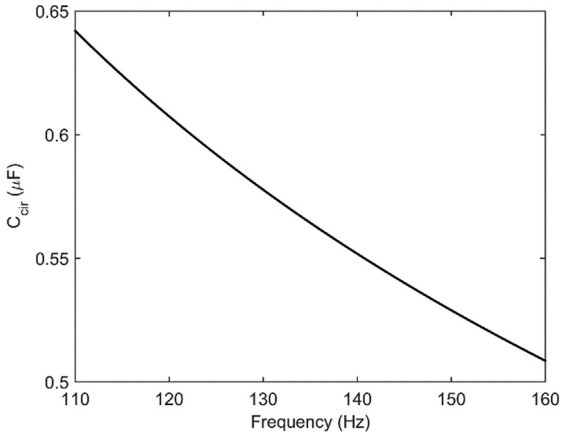

Fig. 5. Equivalent external capacitor capacitance C_{cir} corresponding to X_{cir} in Fig. 4(b).

Table 1
Properties of the bimorph beam harvester in experiments.

Property	Symbol	Value
Length	L	64.30 mm
Width	b	10.01 mm
Brass thickness	t_s	0.50 mm
PSI-5A thickness	t_p	0.13 mm
Brass density	ρ_s	8740 kg/m^3
PSI-5A density	ρ_p	7800 kg/m^3
Brass modulus	Y_s	101 GPa
PSI-5A modulus	Y_p^E	66 GPa
PSI-5A dielectric constant	K_3^T	1800
PSI-5A strain constant	d_{31}	-190×10^{-12} m/V
Mechanical damping ratio	ζ	0.0115
Base acceleration	a	0.5 m/s^2

by an accelerometer (PCB 356A17, PCB Piezotronics Inc.) as the feedback to the close-loop control system. The entire test system was run and controlled by a Laptop. Fig. 6 (c) shows the close-up view of the AC-DC interface circuit, which consists of a full bridge rectifier of four Schottky 1 N5817 Diodes and a smoothing capacitor of 210 μF.

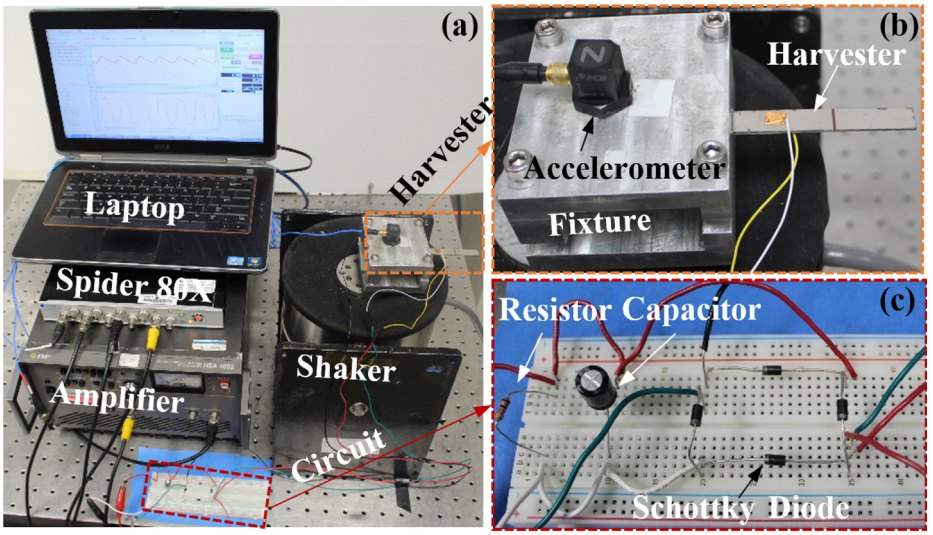

Fig. 6. Experimental setup: (a) overall setup; (b) piezoelectric energy harvester; (c) AC-DC interface circuit.

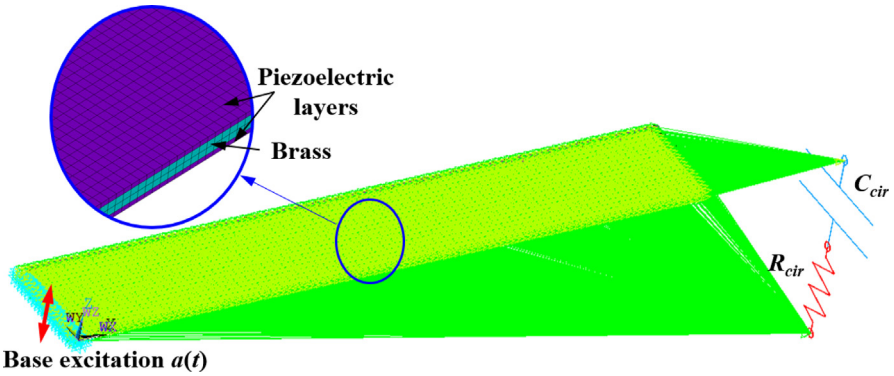

Fig. 7. ANSYS model of the bimorph beam energy harvester with an external equivalent linear circuit.

Fig. 7 shows the parametric finite element model of the bimorph harvester established in ANSYS through APDL. The substrate beam was modeled by the three-dimensional (3D) solid structural element Solid 45 with eight nodes, each of which has three degrees of freedom. The Solid 5 element with eight nodes was used to model the piezoelectric layers with one voltage degree at each node in additional to the other three mechanical degrees of freedom. Both the equivalent circuit capacitance and resistance were simulated by the Circuit 94 element that has two nodes and can interface with piezoelectric element. The model is composed of 7042 elements determined by a convergence test including 3520 structural elements, 3520 piezoelectric elements and 2 circuit elements. The voltage DOF coupling between the piezoelectric and circuit elements is represented by the green lines. Due to the large number of the lines, graphically the lines as a whole appear to be two green areas instead. The composite beam is of a cantilever configuration with one end free and the other end fixed to a vibrating base. The harmonic analysis was conducted on the developed model under the base acceleration excitation of 0.5 m/s^2.

In addition to the experimental and FE results, analytical results were also obtained by an integrated analytical method based on two validated models developed by Shu and Lien in [37] and Liao and Sodano in [44], respectively. This integrated method will be denoted by "Shu/Liao" for the rest of this paper. First, the effective system parameters such as M, C, K, θ, C_p, D of a fully-covered symmetric bimorph beam harvester were given by Liao and Sodano [44] in closed-form as:

$$M = \left(\rho_s t_s + 2\rho_p t_p\right) b$$

$$K = \left[1.0302 Y_s \left(\frac{t_s^3}{L^4}\right) + 2.0604 Y_p^E \left(\frac{3t_s^2 t_p + 6t_s t_p^2 + 4t_p^3}{L^4}\right)\right] b$$

$$\theta = -2.753 d_{31} Y_p^E b \left(\frac{t_s + t_p}{\sqrt{L^3}} \right)$$

$$C_p = 2K_3^S \varepsilon_0 b \left(\frac{L}{t_p} \right)$$

$$D = -0.783 b \left(2\rho_p t_p + \rho_s t_s \right) \sqrt{L} \tag{24}$$

where the physical quantities associated with the symbols are given in Table 1 and $\varepsilon_0 = 8.85 \times 10^{-12}$ is the permittivity of free space of the piezoelectric material. Then the harvested power was determined using the formulas developed by Shu and Lien: Eq. (8) for SEH [37].

4. Results and discussions

Experiments were first conducted on the harvester directly connected with various resistive loads instead of the AC-DC interface circuit and its power was measured and compared to analytical and ANSYS results. This served as a "safety" measure to ensure the energy harvester was working properly, and the values in Table 1 were close to the true values. Fig. 8(a) shows the analytical results from Liao and Sodano's model [44], and 8(b) shows the results from ANSYS coupled-field simulations. The experimental results are shown in Fig. 8(c), which were obtained by performing frequency sweep tests with the harvester connected to a load resistor of different values. The analytical and ANSYS results match well except that the analytical results have a small frequency shift of about 0.5 Hz to the left. This is mostly due to the fact that the analytical model is based on the Euler-Bernoulli beam theory and considers only one vibration mode; while the FE model describes the continuous, physical system more accurately by including the first 80 modes. With reference to the ANSYS results, the experimental peak power is off by +4.03%, +5.02%, +1.99%, −1.87%, −1.92% for the load resistances of 5.1 kΩ, 8 kΩ, 13 kΩ, 20 kΩ, 30 kΩ, respectively. At a lower power level, the discrepancy became larger at 17.65% and −6.58% for the load resistances of 1 kΩ and 150 kΩ, respectively. Overall, in this case of a resistive interface circuit, ANSYS was able to simulate the power behavior of the system accurately, and the results supported the parameter values in Table 1 before experiments with the AC-DC interface circuit.

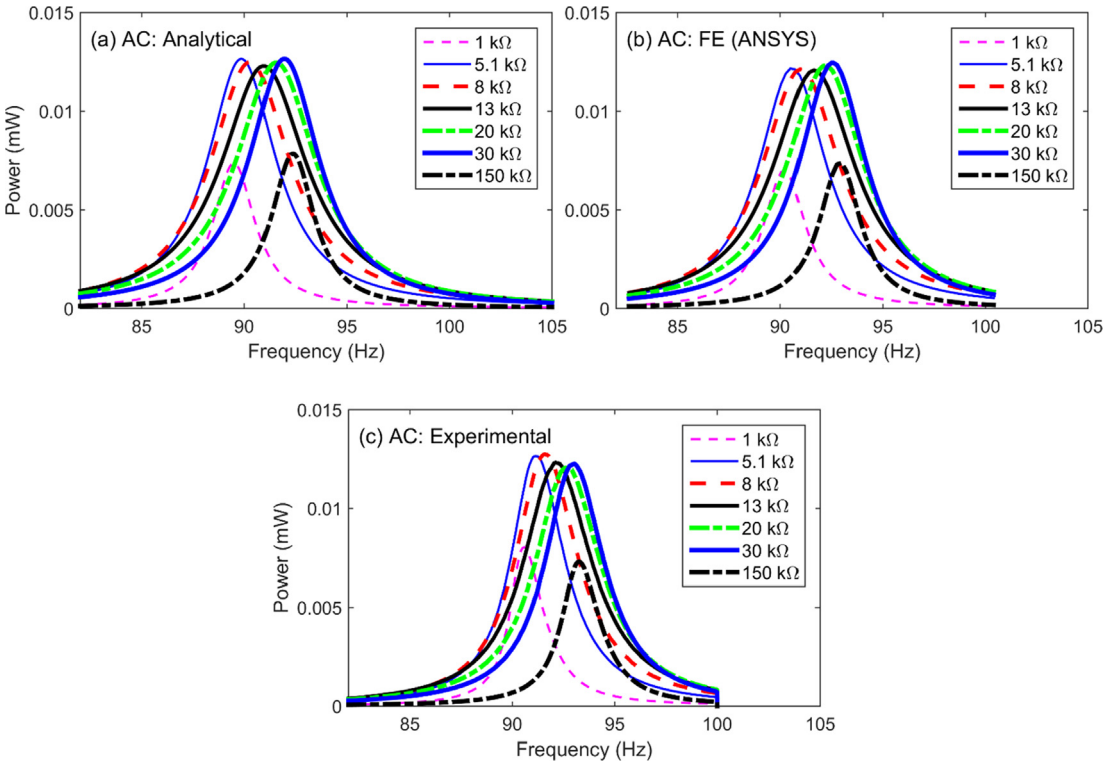

Fig. 8. AC power vs. excitation frequency of the bimorph energy harvester connected to a resistive (AC) interface circuit. (a) Analytical; (b) ANSYS; (c) Experimental. Base excitation, a = 0.5 m/s^2.

The experimental results of the harvester connected with the AC-DC interface circuit are presented in Fig. 9. During the experiments, a harmonic base excitation of 0.5 m/s^2 at a particular frequency was exerted and then the DC voltage over the load resistance was measured. This was repeated for excitation frequency ranging from 86 Hz to 98 Hz. The FE (ANSYS) results were obtained by using the proposed equivalent circuit method. Since the harvester is of a simple structure for which analytical models are available, analytical results are also included for comparison. It can be seen that there is a noticeable frequency shift of about 0.5 between the analytical and FE results, just as for the AC results. The FE and experimental curves follow each other well but the measured data are smaller than the simulation results over the entire frequency range of interest for different resistive loads. It appears that the measured voltage frequency responses slightly bend to the left hand side because of the soft nonlinearities of the beam structure and the AC-DC rectify circuit. The peak voltage difference is 0.1025 V, 0.1166 V, 0.1089 V, 0.1200 V for the load resistance of R = 8 kΩ, 13 kΩ, 20 kΩ, 30 kΩ, respectively. This difference was mostly caused by the voltage drop over the full-bridge rectifier in the experiments, which was not considered in the analytical solution and FE numerical simulations. This could be observed from the measured voltage time history responses over the piezoelectric elements and the resistive load, as plotted in Fig. 10(a). The thin blue line represents the voltage v_p over the piezoelectric elements, i.e., before the rectifier while the thick red line represents the voltage v_L over the load resistance (and smoothing capacitor), i.e., after the rectifier. The voltage v_L appears to be a "perfect" DC signal in this graph but a zoom-in view in Fig. 10(b) reveals small ripples as a result of the filtering effect of the smoothing capacitor. For an ideal rectification, the peak voltage of v_p is equal to v_L. However, the diodes in the rectifier induces forward voltage drops, resulting an overall voltage drop over the rectifier. To study voltage drop due to the rectifier circuit, additional experiments were

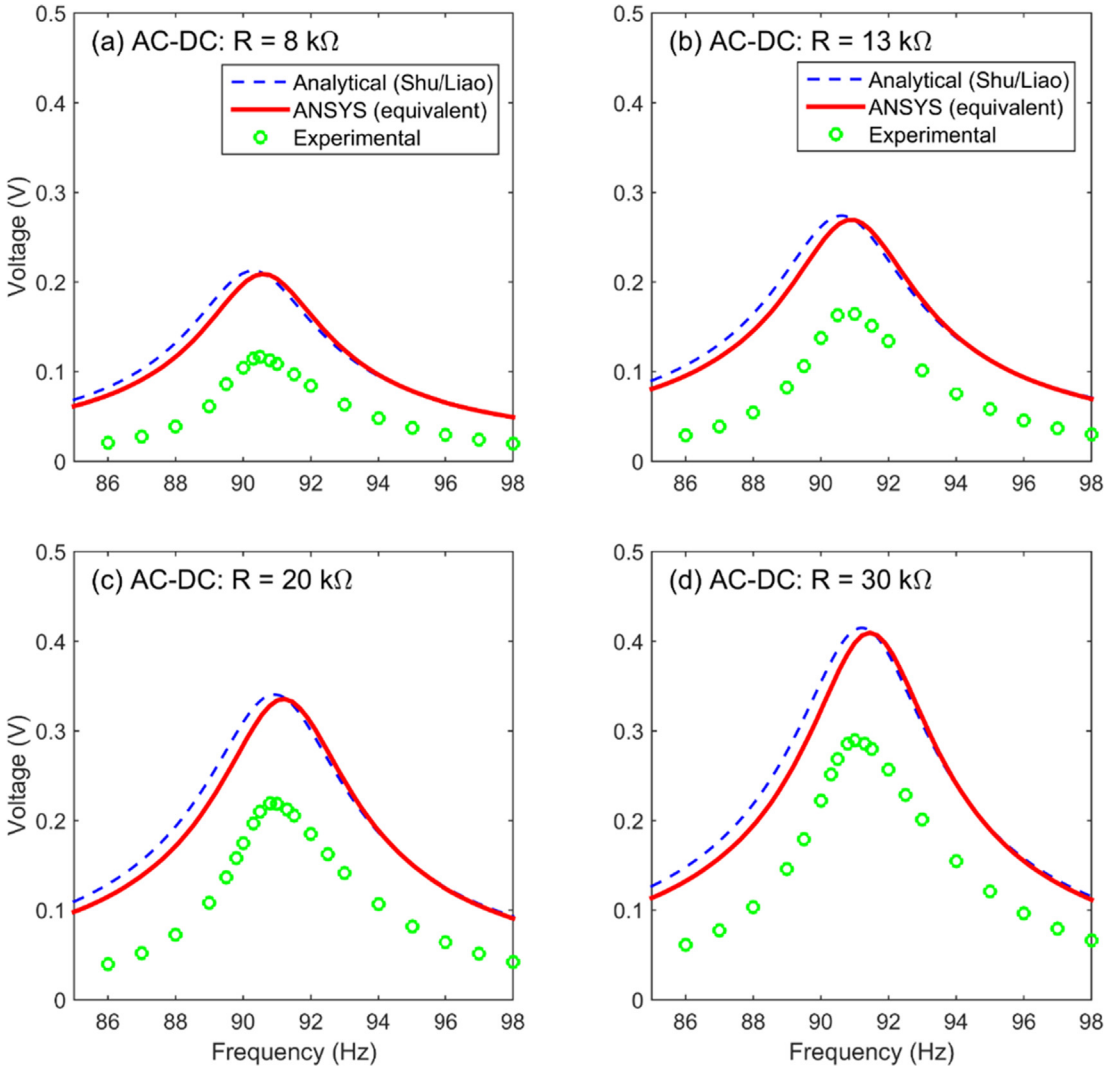

Fig. 9. RMS voltage vs. excitation frequency of the bimorph energy harvester connected to a standard AC-DC (SEH) interface circuit with various load resistance. (a) R = 8 kΩ, (b) R = 13 kΩ, (c) R = 20 kΩ, (d) R = 30 kΩ. Base excitation, a = 0.5 m/s^2.

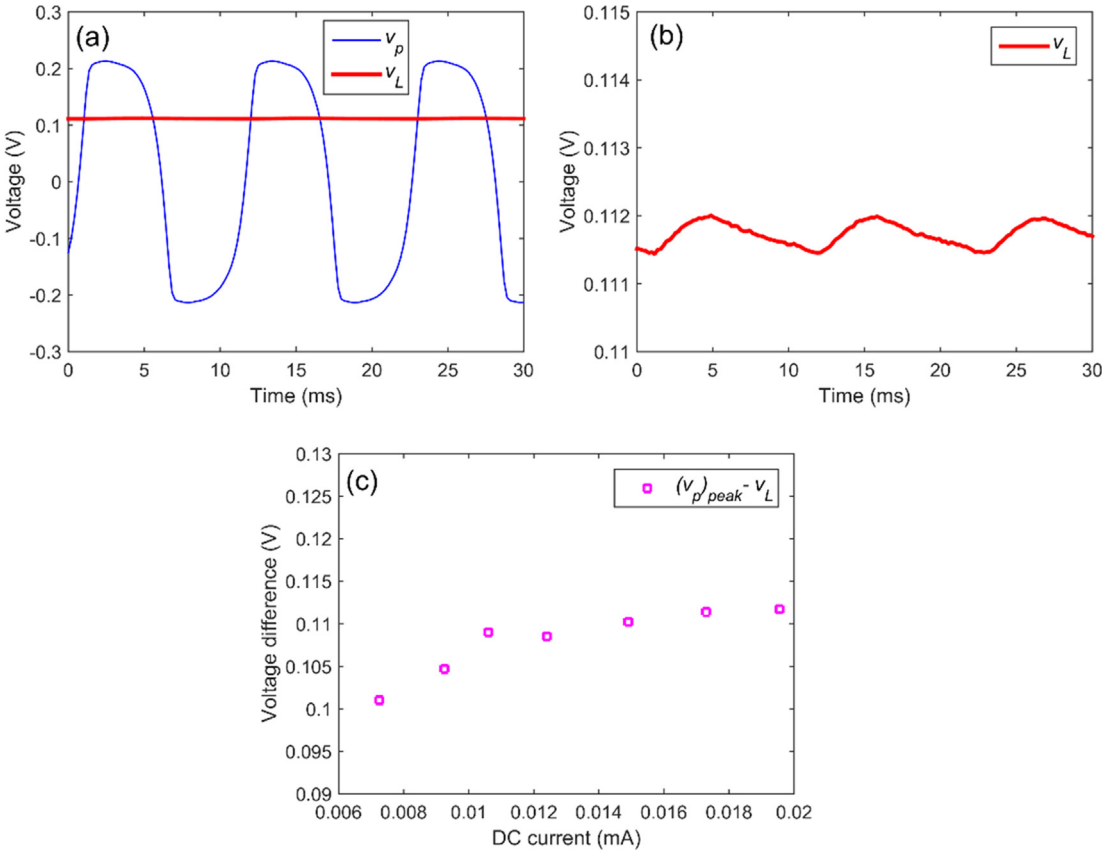

Fig. 10. Voltage drop over the full bridge rectifier. (a) Voltages across the piezoelectric elements v_p and load resistance v_L; (b) zoomed-in view of the voltage signal over the load resistance; (c) voltage difference vs. DC current in the circuit.

conducted to measure the voltage difference at various DC current level. The experimentally measured voltage drop of the rectifier circuit are plotted in Fig. 10(c) against different current level. Over the test current range, the voltage drop generally increased with the current and the average drop was about 0.108 V. This trend is consistent with the property of diodes that the forward voltage drop should increase as the current increases. It is worthwhile to point out that the voltage drop of 0.108 V (over two diodes when the circuit is conducting) appears to be much lower than typical values for forward voltage drop such as 0.45 V, 0.6 V and 0.7 V. This is because that Schottky diodes have a lower forward voltage drop than that of most commonly used types of diodes. In addition, those typical values are usually rated at a much higher current, e.g., 1A, while the current in the experiments was much lower, less than 0.1 mA. In all, it can be concluded that the discrepancy between the FE and experimental results is mostly due to the voltage drop or loss in the rectifier. Note that in addition to the voltage drop over the rectifier, there are other losses as well, for example, dielectric loss in the PZT material and the loss due to parasitic resistance of electrical components. But in this case, their effect does not appear to be as significant as that of the voltage drop of the rectifier. In summary, the results appear to support that the equivalent circuit method for AC-DC simulations is capable of predicting the system behavior satisfactorily once the effect of voltage drop is added into the FE results.

To further demonstrate and validate the capability of this proposed method for simulation studies of AC-DC interfaced PEHs, more experiments were conducted. The harvester was excited at the same, single frequency 91 Hz while the load resistance was varied. The voltage over the load resistance was measured directly, from which the power was computed. The experimental results are plotted in Fig. 11 and indicated by the green circles. The dashed blue line and red line with diamond markers in Fig. 11(a) are the analytical and finite element results, respectively. Again, both the analytical and numerical results do not consider the loss in the actual circuit and "overestimate" the output DC voltage, resulting in a voltage offset graphically. Based on the results in Fig. 10, a voltage offset of 0.108 V (average voltage drop across the rectifier) is applied to the ANSYS results, yielding the "adjusted" voltage results indicated by the red dash-dotted line with triangle markers. It can be seen that once the effect of voltage drop of the rectifier is included, the adjusted FE voltage results are in good agreement with the experimental ones, off by less than 4%. The associated FE power results, shown in Fig. 11(b), are off by less than 10% of the experimental ones. Fig. 11(b) shows that the actual peak RMS power is about 50% of that predicted by the analytical and FE simulations without considering the loss in the circuit. In addition, this optimal resistance at the excitation frequency of 91 Hz is predicted to be around 15 kΩ by the FE method (without the voltage adjustment), while it is about 38 kΩ by

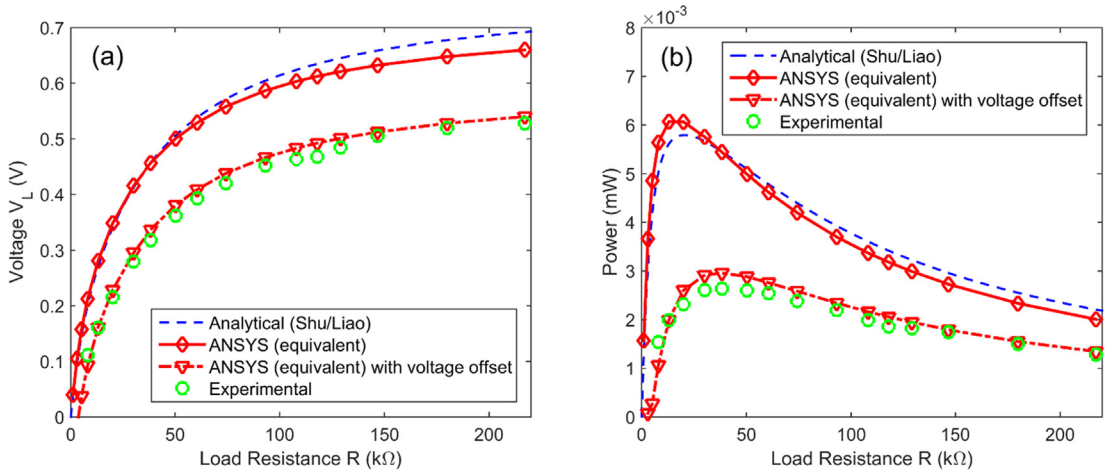

Fig. 11. (a) RMS voltage and (b) RMS power of the bimorph energy harvester connected to a standard AC-DC (SEH) interface circuit with various load resistance, at a single excitation frequency of 91 Hz. Base excitation, a = 0.5 m/s^2.

experimental results. On the other hand, once the voltage drop is considered and included for adjustment, the FE method is able to model the system behavior reasonably well.

Finally, it is worthwhile to point out that analytical results were available and used as a complementary validation method for the bimorph harvester due to its simplicity in structure. However, practical applications often require a more complex structure for which an analytical solution is not available. In that case, the FE simulations become the only viable option. In addition, the analytical results were obtained based on the single-mode assumption. Specifically, the effective SDOF system quantities given in Eq. (24) were determined by assuming the structural response was dominated by the first vibration mode of the system. However, the actual structural response is the summation of all the modes of the system. On the other hand, the FE model provides a more accurate description of the physical system by using 3-D solid elements and including a large number of structural modes. Thus, it is expected there is some difference between the analytical and FE results, for example, the frequency shift shown in Figs. 8 and 9. If the vibration frequency is away from the resonance or the damping increases, the contribution from the other modes grows larger. In this case, the single-mode assumption becomes less accurate and the actual SDOF parameters such as M, C, K, etc. will deviate from the expressions given in Eq. (24). In short, the analytical method considers only one mode and assumes that M, C, K, etc. are always the same (based on the single mode); while the FE model is able to include and adjust the contribution from the other modes accordingly. Moreover, we would like to clarify that the proposed equivalent linear circuit method is an equivalent representation of the circuit only. Although its derivation was based on a general SDOF model subjected to harmonic excitation, it did not make any assumption on how the SDOF system parameters such as M, C, K, etc. were obtained exactly. The equivalent circuit representation only depends on the electrical load, internal capacitance, and excitation frequency. When it is coupled with the FE package or formulation, it implies that multiple modes are considered, providing a better estimate of M, C, K, etc.

5. Application examples

5.1. Application in FE packages

As an application example, this proposed equivalent linear circuit method is used in this section to study the influence of harvester geometry on energy harvesting performance, specifically, the triangular shape compared to the regular rectangular shape. There are few similar studies conducted by researchers in the past. For instance, it was suggested by Roundy et al. [47] that an increasingly trapezoidal shaped profile helps distribute the mechanical strain more evenly, as opposed to a rectangular profile that has an almost linearly decreasing strain distribution along the beam. Mateu and Moll [48] performed a detailed study of strain distribution of triangular shaped cantilevers and derived the analytical expression of harvested power for energy harvesting using shoe inserts. However, they used the static deflection and did not include the backward coupling to the structure from the electrical dynamics. Sameh et al. [49] developed a mathematical model to describe the dynamics of a trapezoidal unimoph piezoelectric cantilever subjected to a harmonic force at the free end, and concluded that the shape should be as truncated as possible in order to increase the harvested power. Recently, Muthaif and Nordian [50] also derived a model to estimate the voltage output of a trapezoidal-shaped piezoelectric cantilever, and they showed that the output voltage increased as the beam width at the tip reduced, while the beam length and the beam width at the fixed end kept unchanged. In other words, the triangular configuration yielded the highest voltage output. In these studies, the energy harvesting interface circuit was resistive for simplicity. The natural frequency of the system was allowed to change

freely, which may be unrealistic in many situations where the natural frequency needs to match the excitation frequency source. In our study, the more practical AC-DC interface circuit is used. In addition, as an important aspect that did not receive much deserved attention, the effect of electromechanical coupling is investigated. Note that in this comparison study, the voltage drop of the rectifier is not considered. In other words, the circuitry is assumed to be ideal without loss. This voltage drop depends on the type of diodes and amount of current in the circuit, which is important to be determined and included in the actual design study for practical applications.

There were two groups of PEHs being investigated, with each grouping consisting a rectangular PEH and a triangular PEH. The important difference between the two groups is that group 1 PEHs have lower electromechanical coupling than that of group 2 PEHs. Table 2 lists the properties of the two rectangular harvesters in groups 1 and 2, respectively. The PZT material in the groups are MFC and PSI-5H, respectively. Within each group, for a fair comparison between the rectangular PEH and its triangular counterpart, the dimensions of the isosceles triangular PEH were configured in a way such that it had the same thickness and volume as the rectangular PEH harvester. In addition, the first natural frequency was also kept the same, i.e. 141.3 Hz. As mentioned, practically, there could a target dominant excitation frequency for the PEH in the actual working environment. This is an important constraint but tends to be overlooked in most optimization or design studies. As a result of the volume and natural frequency constraints, the width and height of the triangular PEHs have been determined as shown in Table 3. The ANSYS model of the PEH is shown in Fig. 12. A convergence test was performed to the mesh before the harmonic power analysis was conducted.

The equivalent linear circuit method for AC-DC interface circuit is applied to the two groups. The base-motion excitation is 1 g and the damping ratio is 0.019. Fig. 13 plots the harvested power of group 1 PEHs versus excitation frequency at various load resistance, with the rectangular PEH in Fig. 13(a) and the triangular one in Fig. 13(b), respectively. It can be seen that the triangular harvester has a much higher peak power than the rectangular harvester, an increase of about 29% from 0.715 mW to 0.923 mW. In addition, the power curves appear to spread out more, which is an indication of stronger electromechanical coupling. A simple way to "experimentally" assess the coupling of a system is to utilize the short-circuit natural frequency $(\omega_n)_{SC}$ and open-circuit natural frequency $(\omega_n)_{OC}$ as

Table 2
Properties of the rectangular bimorph beam harvesters in Section 4.

Property	Symbol	Rectangular PEH #1	Rectangular PEH #2
Length	L	66.62 mm	66.62 mm
Width	b	9.72 mm	9.72 mm
Brass thickness	t_s	1.042 mm	0.76 mm
PZT thickness	t_p	0.25 mm	0.26 mm
Brass density	ρ_s	8740 kg/m^3	8740 kg/m^3
PZT density	ρ_p	7500 kg/m^3	7800 kg/m^3
Brass modulus	Y_s	101 GPa	101 GPa
PZT modulus	Y_p^E	30.34 GPa	66 GPa
PZT dielectric constant	K_3^T	1700	1800
PZT strain constant	d_{31}	-170×10^{-12} m/V	-320×10^{-12} m/V

Table 3
Geometry of the triangular bimorph beam harvesters in Section 4.

Property	Symbol	Triangular PEH #1	Triangular PEH #2
Length (height)	L	95.5 mm	95.9 mm
Width (base)	b	13.6 mm	13.5 mm

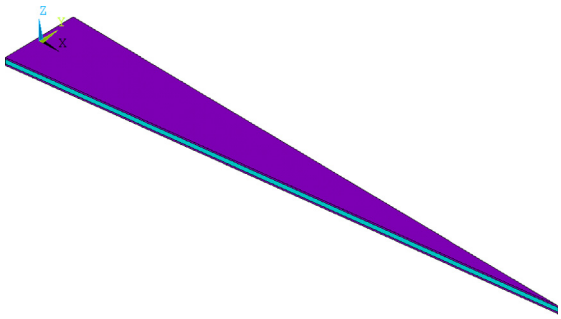

Fig. 12. ANSYS model of the triangular bimorph beam energy harvester.

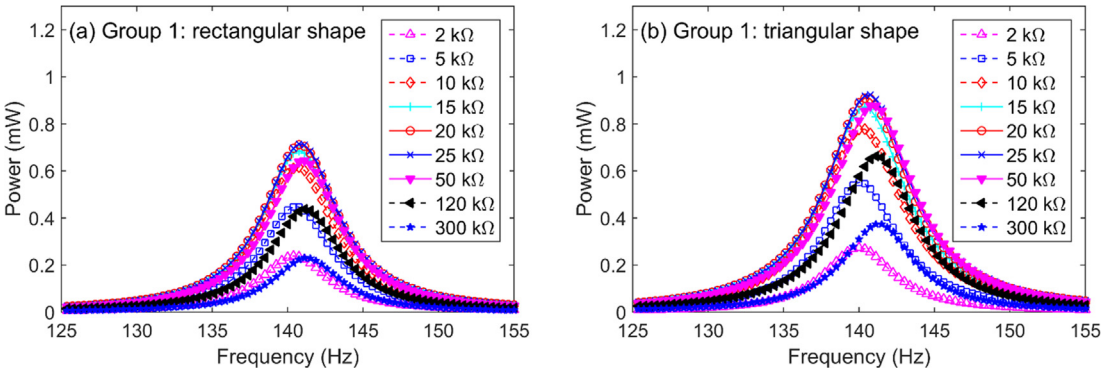

Fig. 13. Harvested RMS power versus excitation frequency at various resistances for harvesters connected with the standard AC-DC interface circuit for group 1 PEHs: (a) rectangular, (b) triangular. Base motion excitation, 1 *g*; damping ratio, 0.019.

$$k^2 = \frac{(\omega_n^2)_{OC} - (\omega_n^2)_{SC}}{(\omega_n^2)_{SC}}. \tag{25}$$

ANSYS simulations showed that the rectangular harvester had short-circuit and open-circuit natural frequencies of 140.2 Hz and 141.3 Hz, respectively. Based on these values, Eq. (25) gives a coupling coefficient of 0.0158, close to the value of 0.0151 obtained from the analytical model by Liao and Sodano [44]. On the other hand, the triangular harvester has short-circuit and open-circuit natural frequencies of 139.7 Hz and 141.3 Hz, respectively, from which the coupling coefficient is determined to be 0.0230. Therefore, the coupling coefficient increases significantly by about 46%. As pointed out by Roundy et al. [47], a triangular shaped profile helps distribute the mechanical strain more evenly, and more PZT material is located in the high stress area. This results in a higher energy conversion efficiency, an increased coupling coefficient, and more harvested power. Therefore, what is shown in Fig. 13 is consistent with the common understanding that stronger electromechanical coupling is desirable for improving power performance: higher power output and broader bandwidth.

However, in addition to electromechanical coupling, the maximum power of a harvester depends on other aspects of the system as well and the triangular shape does not always serve as a solution for enhanced power performance. To illustrate this point, Fig. 14 shows the power curves of group 2 harvesters, which have higher coupling than their group 1 counterparts. A quick inspection of Fig. 14(a) and (b) reveals few main differences. Firstly, the overall maximum harvested power of the triangular PEH is actually lower than that of the rectangular PEH, i.e., about 1.3 mW compared to 1.7 mW, a decrease of 24%. Secondly, the triangular PEH has a broader harvesting frequency bandwidth. Thirdly, the outer profile created by the power curves overlaid together, called power envelope [45], appears to be different too. The triangular PEH has a "M" shaped profile; while the rectangular PEH has a "Λ" shaped profile. The explanation of these observations also starts with an investigation of the difference in electromechanical coupling between the two configurations. For the rectangular PEH, the short-circuit and open-circuit natural frequencies have been found to be 135.0 Hz and 141.3 Hz, respectively, from the ANSYS analysis. This yields a coupling coefficient k^2 = 0.0955, which matches the analytical coupling coefficient k^2 = 0.0976 obtained by using the model by Liao and Sodano [44]. As explained in [43,51], initially, the energy conversion efficiency increases as the coupling increases, yielding more harvested power. However, at the same time, the induced damping due to energy harvesting also increases, resulting in a reduced structural response. As the coupling reaches a critical value, the increased energy conversion efficiency and reduced structural response reach a balance, and the power saturates

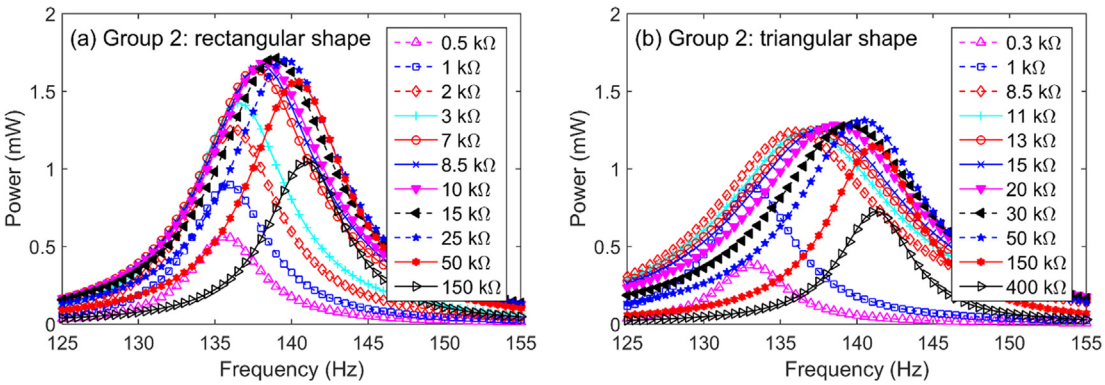

Fig. 14. Harvested power versus excitation frequency at various resistances for harvesters connected with the standard AC-DC interface circuit: (a) rectangular PEH, (b) triangular PEH. Base motion excitation, 1 *g*; damping ratio, 0.019.

at a level called power limit. For energy harvesters with a standard AC-DC interface circuit, the critical coupling has been shown to be a function of damping ratio [42]:

$$\left(k^2\right)_c^{SEH} \approx 6.277\zeta + 10.07\zeta^2. \tag{26}$$

For damping ratio ζ = 0.019, the critical coupling is approximately 0.123. Because the coupling of the rectangular PEH is lower than the critical coupling, the system is defined as weakly coupled. The power limit of the system is not reached, and its power envelope has a "Λ" shape. On the other hand, the triangular PEH has short-circuit and open-circuit natural frequencies 135.0 Hz and 141.3 Hz, respectively, from which the system coupling coefficient is determined to be 0.127. Since the coupling coefficient is greater than the critical coupling coefficient 0.123, the system is strongly coupled. Its power envelope has a "M" shape and the power limit is reached at two locations. In addition, as the coupling increases, the power envelop usually expands [42], which leads to a broader harvesting bandwidth as shown in Fig. 14(b).

However, although it is desirable to have high coupling to harvest more power, the power output is capped by the power limit of a system, which mostly depends on the mechanical aspect of the system. Mathematically, the power limit has been obtained as [42]:

$$P_{\lim} = \frac{D^2A^2}{\sqrt{MK}}\frac{1}{8\zeta}, \tag{27}$$

where M, K, D are the effective mass, stiffness, input mass of the system, respectively [44]. A is the amplitude of the harmonic base-motion acceleration. As the system geometry changes, these effective mechanical quantities also change. In this particular case, changing the beam shape from rectangular to triangular increases the coupling coefficient by more than 25%, i.e., from 0.0955 to 0.127, which extends the harvesting bandwidth and is extremely desirable for broadband energy harvesting applications. However, doing this also reduces the system power limit by about 26%.

In summary, this comparison study shows that for beam harvesters of low coupling, e.g., group 1 harvesters, it is beneficial to adopt a triangular profile as it only increases the harvested power but also broadens the energy harvesting bandwidth. However, if the beam harvester already has a relatively high coupling, e.g., group 2 harvesters, adopting a triangular profile might actually decrease the harvested power as a result of power saturation and reduced power limit. The example is used to demonstrate the application of the proposed equivalent linear circuit method for simulations of energy harvesters with rectified circuits, facilitating a system-level coupled-filed analysis. It does not intend to provide a complete optimization study. However, it can be seen that this method opens up opportunities for more detailed optimization studies that consider additional variables, for instance, thickness and length, and other geometrical shapes such as trapezoidal.

5.2. Application in FE formulations

In addition to FE packages that have built-in capabilities of handling linear interface circuits, the equivalent circuit method can also be extended to custom developed FE formulations [22–28] conveniently. As discussed in the Section 1, these formulations were limited to a resistive interface circuit. The proposed method can be utilized here to enable numerical studies of harvesters connected with a standard AC-DC interface circuit. In general, the coupled governing equations in Eq. (1) can be written in a discrete form as:

$$\boldsymbol{M}^{(FE)}\ddot{\boldsymbol{u}}^{(FE)}(t) + \boldsymbol{C}^{(FE)}\dot{\boldsymbol{u}}^{(FE)}(t) + \boldsymbol{K}^{(FE)}\boldsymbol{u}^{(FE)}(t) - \boldsymbol{\theta}^{(FE)}v_p(t) = \boldsymbol{f}^{(FE)}(t), \tag{28}$$

$$\boldsymbol{\theta}^{(FE)T}\boldsymbol{u}^{(FE)}(t) + C_p v_p(t) = q(t). \tag{29}$$

The number of structural DOFs is denoted as N_S,$\boldsymbol{M}^{(FE)}$, $\boldsymbol{K}^{(FE)}$, and $\boldsymbol{C}^{(FE)}$ are the N_S-by-N_S mass, stiffness and damping matrices, respectively, and $\boldsymbol{u}^{(FE)}$, $\boldsymbol{\theta}^{(FE)}$, $\boldsymbol{f}^{(FE)}$ are the N_S-by-1 structural displacement, electromechanical coupling coefficients, and force vectors, respectively. In the case of an AC-DC interface circuit, the interface circuit is equivalently represented and replaced by a resistor and capacitor in series as illustrated in Fig. 1. Through the manipulation of voltage and charge relationships in the circuit, the governing equations are modified to be

$$\boldsymbol{M}^{(FE)}\ddot{\boldsymbol{u}}^{(FE)}(t) + \boldsymbol{C}^{(FE)}\dot{\boldsymbol{u}}^{(FE)}(t) + \boldsymbol{K}^{(FE)}\boldsymbol{u}^{(FE)}(t) + \boldsymbol{\theta}^{(FE)}R_{cir}\dot{q}(t) + \frac{\boldsymbol{\theta}^{(FE)}}{C_{cir}}q(t) = \boldsymbol{f}^{(FE)}(t), \tag{30}$$

$$\left\{\boldsymbol{\theta}^{(FE)}\right\}^T\boldsymbol{u}^{(FE)}(t) - R_{cir}C_p\dot{q}(t) - \left(1 + \frac{C_p}{C_{cir}}\right)q(t) = 0, \tag{31}$$

where R_{cir} and C_{cir} are the equivalent linear circuit resistance and capacitors given in Eqs. (18) and (23), respectively.

6. Conclusions

Based on the equivalent impedance analysis, a method is proposed to realize a full and direct coupled-field simulation in finite element packages and formulations for piezoelectric energy harvesters of complex geometry with a standard AC-DC rectified circuit. The method replaces the nonlinear rectified circuit with an equivalent linear circuit of a resistor and capacitor in series. The impedance of the equivalent linear circuit is extracted from the equivalent electrical impedance that combines the internal capacitance of the piezoelectric elements and the original rectified energy harvesting circuit. The expressions to determine the values of the equivalent linear circuit elements are obtained and explicitly provided as functions of the load resistance, excitation frequency, and internal capacitance.

For validation, the method was applied to a bimorph beam harvester connected with a standard AC-DC rectified circuit, and the results match well with those obtained by using a system-level analytical approach integrated from two analytical models. Experiments were conducted to verify the proposed method and the results were consistently lower than the finite element (also analytical) results mostly due to the voltage drop over the rectifier, which was not considered in the analytical models. Once the voltage drop was considered and included for adjustment, the FE method based on the equivalent linear circuit approach was shown to be capable of modeling the actual system behavior well.

As an application example, the proposed method was implemented in ANSYS to study the energy harvesting performance of a triangular-shaped beam harvester, compared to its rectangular-shaped counterpart with the same thickness, volume and natural frequency. The triangular configuration has a more uniformly-distributed strain and more piezoelectric material lies in the high strain region. As a result, the electromechanical coupling increases and the harvesting frequency bandwidth widens. However, due to this modification, the power limit of the system is also changed. In the case of low coupling, both the harvested power and coupling increase as a result of shape modification. However, if the coupling of the system is not low, though the shape change still leads to a broadened energy harvesting bandwidth, the overall power level could be lower as a result of a reduced power limit. In addition to FE packages that have built-in capabilities of handling linear interface circuits, the idea of integrating this proposed equivalent circuit method into FE formulations was also discussed.

The proposed equivalent linear circuit method has been shown to be a capable and useful tool for facilitating numerical and design studies of PEH systems. It enables a system-level coupled-field simulation of piezoelectric energy harvesters of rectified interface circuit by FE packages and formulations limited to linear circuits, an extremely desirable capability for analysis, design and optimization of complex PEH harvesters.

Lastly, we would like to add a couple of important notes on the limitation and capability of the proposed method. First, the proposed method is based on a harmonic vibration analysis in the frequency domain, and the equivalent linear circuit resistance and capacitance depend on the harmonic excitation frequency. Thus, this method cannot be applied to random vibration problems directly. This poses as an interesting challenge and a great direction to be explored in the future. The second note, which was mentioned previously but is worth being reemphasized here, is that although a simple, fully-covered bimorph beam configuration is used in the paper, this proposed method is capable of handling structures of more complex geometries too. The simply configuration allows obtaining complementary, analytical results for validation purposes in addition to the FE and experimental results, but the proposed method is not limited to this simple configuration. Essentially, this validated method is on the equivalency of linear and nonlinear circuitry for simulations of electromechanically coupled systems, and does not depend on the structural aspect of the system, which can be seen from Eqs. (18) and (23). FE methods have been shown to be capable of modeling the mechanical aspect of electromechanical systems of various geometries accurately [8–28]. Therefore, the method will enable an accurate, system-level FE simulation for linear mechanical systems of complex geometry too.

CRediT authorship contribution statement

Feng Qian: Methodology, Software, Writing - original draft, Investigation. **Yabin Liao:** Conceptualization, Methodology, Writing - original draft, Visualization, Supervision. **Lei Zuo:** Writing - review & editing, Supervision, Project administration. **Phil Jones:** Software, Resources.

Declaration of Competing Interest

The authors declare that they have no known competing financial interests or personal relationships that could have appeared to influence the work reported in this paper.

References

[1] F.K. Shaikh, S. Zeadally, Energy harvesting in wireless sensor networks: A comprehensive review, Renew. Sustain. Energy Rev. 55 (2016) 1041–1054.
[2] H.A. Sodano, D.J. Inman, G. Park, A review of power harvesting from vibration using piezoelectric materials, Shock Vib. 36 (2004) 197–205.
[3] S.P. Beeby, M.J. Tudor, N.M. White, Energy harvesting vibration sources for microsystems applications, Meas. Sci. Technol. 17 (2006) R175–R195.
[4] S.R. Anton, H.A. Sodano, A review of power harvesting using piezoelectric materials (2003–2006), Smart Mater. Struct. 16 (2007) R1–R21.
[5] L. Tang, Y. Yang, C.K. Soh, Toward broadband vibration-based energy harvesting, J. Intell. Mater. Syst. Struct. 21 (2010) 1867–1897.
[6] L. Zuo, X. Tang, Large-scale vibration energy harvesting, J. Intell. Mater. Syst. Struct. 24 (2013) 1405–1430.
[7] C. Wei, X. Jing, A comprehensive review on vibration energy harvesting: Modelling and realization, Renew. Sustain. Energy Rev. 74 (2017) 1–18.

[8] N.G. Elvin, A.A. Elvin, A coupled finite element—circuit simulation model for analyzing piezoelectric energy generators, J. Intell. Mater. Syst. Struct. 20 (2009) 587–595.
[9] V. Vyas, X.Q. Wang, A. Jain, M.P. Mignolet, Nonlinear geometric reduced order model for the response of a beam with a piezoelectric actuator, in: 2015 56th Structures, Structural Dynamics, and Materials Conference (AIAA SciTech), AIAA, 2015, pp. 2015-0692.
[10] M. Zhu, E. Worthington, J. Njuguna, Analyses of power output of piezoelectric energy-harvesting devices directly connected to a load resistor using a coupled piezoelectric-circuit finite element method, IEEE Trans. Ultrason. Ferroelectr. Freq. Control 56 (2009) 1309–1317.
[11] Y. Kuang, M. Zhu, Design study of a mechanically plucked piezoelectric energy harvester using validated finite element modelling, Sens. Actuators, A. 263 (2017) 510–520.
[12] Y. Yang, L. Tang, Equivalent circuit modeling of piezoelectric energy harvesters, J. Intell. Mater. Syst. Struct. 20 (2009) 2223–2235.
[13] M. Arafa, W. Akl, A. Aladwani, O. Aldraihem, A. Baz, Experimental Implementation of a Cantilevered Piezoelectric Energy Harvester with a Dynamic Magnifier, in: Proc. SPIE 7977, Active and Passive Smart Structures and Integrated Systems 2011, 79770Q (27 April 2011)
[14] Y. Bai, P. Tofel, Z. Hadas, J. Smilek, P. Losak, P. Skarvada, R. Macku, Investigation of a cantilever structured piezoelectric energy harvester used for wearable devices with random vibration input, Mech. Syst. Sig. Process. 106 (2018) 303–318.
[15] F. Qian, T.B. Xu, L. Zuo, Material equivalence, modeling and experimental validation of a piezoelectric boot energy harvester, Smart Mater. Struct. 28 (2019) 075018.
[16] G. Wang, J. Tan, Z. Zhao, S. Cui, H. Wu, Mechanical and energetic characteristics of an energy harvesting type piezoelectric ultrasonic actuator, Mech. Syst. Sig. Process. 128 (2019) 110–125.
[17] X. Li, D. Upadrashta, K. Yu, Y. Yang, Y, Analytical modeling and validation of multi-mode piezoelectric energy harvester, Mech. Syst. Sig. Process. 124 (2019) 613–631.
[18] D. Zhu, S. Beeby, J. Tudor, N. White, N. Harris, Improving output power of piezoelectric energy harvesters using multilayer structures, Procedia Eng. 25 (2011) 199–202.
[19] J. Park, S. Lee, B.M. Kwak, Design optimization of piezoelectric energy harvester subject to tip excitation, J. Mech. Sci. Technol. 26 (2012) 137–143.
[20] S. Lee, B.D. Youn, A new piezoelectric energy harvesting design concept: multimodal energy harvesting skin, IEEE Trans. Ultrason. Ferroelectr. Freq. Control 58 (2011) 629–645.
[21] L. Zhou, J. Sun, X. Zheng, S. Deng, J. Zhao, S. Peng, Y. Zhang, X. Wang, H. Cheng, A model for the energy harvesting performance of shear mode piezoelectric cantilever, Sens. Actuators, A 179 (2012) 185–192.
[22] C. De Marqui Junior, A. Erturk, D.J. Inman, An electromechanical finite element model for piezoelectric energy harvester plates, J. Sound Vib. 327 (2009) 9–25.
[23] A. Kumar, A. Sharma, R. Kumar, R. Vaish, V.S. Chauhan, Finite element analysis of vibration energy harvesting using lead-free piezoelectric materials: A comparative study, J. Asian Ceram. Soc. 2 (2) (2014) 139–143.
[24] I. Fattahi, H. Mirdamadi, Novel composite finite element model for piezoelectric energy harvesters based on 3D beam kinematics, Compos. Struct. 179 (2017) 161–171.
[25] J. Ramírez, C. Gatti, S. Machado, M. Febbo, An experimentally validated finite element formulation for modeling 3D rotational energy harvesters, Eng. Struct. 153 (2017) 136–145.
[26] X.Q. Wang, Y. Liao, M.P. Mignolet, Nonparametric uncertainty analysis of piezoelectric vibration energy harvesters by finite-element-level maximum entropy approach, ASCE-ASME J. Risk Uncertainty Eng. Syst., Part B Mech. Eng. (2020), in press.
[27] Y. Amini, H. Emdad, M. Farid, An accurate model for numerical prediction of piezoelectric energy harvesting from fluid structure interaction problems, Smart Mater. Struct. 23 (2014) 095034.
[28] S. Ravi, A. Zilian, Simultaneous finite element analysis of circuit-integrated piezoelectric energy harvesting from fluid-structure interaction, Mech. Syst. Sig. Process. 114 (2019) 259–274.
[29] G.K. Ottman, H.F. Hofmann, A.C. Bhatt, G.A. Lesieutre, Adaptive piezoelectric energy harvesting circuit for wireless remote power supply, IEEE Trans. Power Electron. 17 (2002) 669–676.
[30] D. Guyomar, A. Badel, E. Lefeuvre, C. Richard, Toward energy harvesting using active materials and conversion improvement by nonlinear processing, IEEE Trans. Ultrason. Ferroelectr. Freq. Control. 52 (2005) 584–595.
[31] C. Richard, D. Guyomar, D. Audigier, H. Bassaler, Enhanced semi-passive damping using continuous switching of a piezoelectric device on an inductor, In: 2000 Smart structures and materials, SPIE, 2000, pp. 3989 288–299.
[32] Y.K. Ramadass, A.P. Chandrakasan, An efficient piezoelectric energy harvesting interface circuit using a bias-flip rectifier and shared inductor, IEEE J. Solid-State Circuits 45 (2010) 189–204.
[33] D. Motter, J.V. Lavarda, F.A. Dias, S.D. Silva, Vibration energy harvesting using piezoelectric transducer and non-controlled rectifiers circuits, J. Braz. Soc. Mech. Sci. Eng. 34 (2012) 378–385.
[34] A.A. Mustapha, S.L. Kok, N.M. Ali, Piezoelectric energy harvesting rectifying circuits comparison, ARPN J. Eng. Appl. Sci. 11 (2016) 6361–6365.
[35] J. Dicken, P.D. Mitcheson, I. Stoianov, E.M. Yeatman, Power-extraction circuits for piezoelectric energy harvesters in miniature and low-power applications, IEEE Trans. Power Electron. 27 (2012) 4514–4529.
[36] G.D. Szarka, B.H. Stark, S.G. Burrow, Review of power conditioning for kinetic energy harvesting systems, IEEE Trans. Power Electron. 27 (2012) 803–815.
[37] Y.C. Shu, I.C. Lien, Analysis of power outputs for piezoelectric energy harvesting systems, Smart Mater. Struct. 15 (2006) 1499–1502.
[38] J. Liang, W.H. Liao, Impedance modeling and analysis for piezoelectric energy harvesting systems, IEEE/ASME Trans. Mechatron. 17 (2012) 1145–1157.
[39] N.G. Elvin, A.A. Elvin, A coupled finite element-circuit simulation model for analyzing piezoelectric energy generators, J. Intell. Mater. Syst. Struct. 20 (2008) 587–595.
[40] P.H. Wu, Y.C. Shu, Finite element modeling of electrically rectified piezoelectric energy harvesters, Smart Mater. Struct. 24 (2012) 094008.
[41] C. Cheng, Z. Chen, H. Shi, Z. Liu, Y. Xiong, System-level coupled modeling of piezoelectric vibration energy harvesting systems by joint finite element and circuit analysis, Shock Vib. 2016 (2016) 2413578.
[42] Y. Liao, J. Liang, Maximum power, optimal load, and impedance analysis of piezoelectric vibration energy harvesters, Smart Mater. Struct. 27 (2018) 075053.
[43] Y. Liao, J. Liang, Unified modeling, analysis and comparison of piezoelectric vibration energy harvesters, Mech. Syst. Sig. Process. 123 (2019) 403–425.
[44] Y. Liao, H.A. Sodano, Model of a single mode energy harvester and properties for optimal power generation, Smart Mater. Struct. 17 (2008) 065026.
[45] N.W. Hagood, W.H. Chung, A. Von Flotow, Modeling of piezoelectric actuator dynamics for active structural control, J. Intell. Mater. Syst. Struct. 1 (1990) 327–354.
[46] I.C. Lien, Y.C. Shu, Array of piezoelectric energy harvesting by the equivalent impedance approach, Smart Mater. Struct. 21 (2012) 082001.
[47] S. Roundy, E.S. Leland, J. Baker, E. Carleton, E. Reilly, E. Lai, B. Otis, J.M. Rabaey, P.K. Wright, V. Sundararajan, Improving power output for vibration-based energy scavengers, Pervasive Computing IEEE 4 (1) (2005) 28–36.
[48] L. Mateu, F. Moll, Optimum piezoelectric bending beam structures for energy harvesting using shoe inserts, J. Intell. Mater. Syst. Struct. 16 (2005) 835–845.
[49] S.B. Ayed, F. Najar and A. Abdelkefi, Shape improvement for piezoelectric energy harvesting applications. Paper presented at the 3rd International Conference on Signals, Circuits and Systems (SCS), 2009
[50] A.G.A. Muthaif, N.H.D. Nordin, Optimal piezoelectric beam shape for single and broadband vibration energy harvesting: Modeling, simulation and experimental results, Mech. Syst. Sig. Process. 54–55 (2015) 417–426.
[51] Y. Liao, Analysis of power and efficiency of piezoelectric vibration energy harvesters through an impedance plot, J. Intell. Mater. Syst. Struct. 30 (2019) 3036–3055.